Clinical Science (2016) **130**, 1221–1236 doi: 10.1042/CS20160064

Original Paper

Local inhibition of elastase reduces EMILIN1 cleavage reactivating lymphatic vessel function in a mouse lymphoedema model

Eliana Pivetta*, Bruna Wassermann*, Lisa Del Bel Belluz*†, Carla Danussi*‡, Teresa Maria Elisa Modica*, Orlando Maiorani*, Giulia Bosisio*, Francesco Boccardo§, Vincenzo Canzonieri‖, Alfonso Colombatti* and Paola Spessotto*

*Experimental Oncology 2, Department of Translational Research, CRO-IRCCS, National Cancer Institute, 33081, Aviano, Italy
†Department of Cell and Molecular Biology, Karolinska Institutet, SE-171 77 Stockholm, Sweden
‡Human Oncology and Pathogenesis Program, Memorial Sloan Kettering Cancer Center, New York, NY 10065, U.S.A.
§Department of Surgery – Unit of Lymphatic Surgery, IRCCS S. Martino University Hospital – IST, National Institute for Cancer Research, University of Genoa, 16132 Genoa, Italy
‖Division of Pathology, Department of Translational Research, CRO-IRCCS, National Cancer Institute, 33081, Aviano, Italy

Abstract

Lymphatic vasculature critically depends on the connections of lymphatic endothelial cells with the extracellular matrix (ECM), which are mediated by anchoring filaments (AFs). The ECM protein EMILIN1 is a component of AFs and is involved in the regulation of lymphatic vessel functions: accordingly, *Emilin1*$^{-/-}$ mice display lymphatic vascular morphological alterations, leading to functional defects such as mild lymphoedema, lymph leakage and compromised lymph drainage. In the present study, using a mouse post-surgical tail lymphoedema model, we show that the acute phase of acquired lymphoedema correlates with EMILIN1 degradation due to neutrophil elastase (NE) released by infiltrating neutrophils. As a consequence, the intercellular junctions of lymphatic endothelial cells are weakened and drainage to regional lymph nodes is severely affected. The local administration of sivelestat, a specific NE inhibitor, prevents EMILIN1 degradation and reduces lymphoedema, restoring a normal lymphatic functionality. The finding that, in human secondary lymphoedema samples, we also detected cleaved EMILIN1 with the typical bands of an NE-dependent pattern of fragmentation establishes a rationale for a powerful strategy that targets NE inhibition. In conclusion, the attempts to block EMILIN1 degradation locally represent the basis for a novel 'ECM' pharmacological approach to assessing new lymphoedema treatments.

Key words: EMILIN1, extracellular matrix, human lymphoedematous tissue, neutrophil elastase, secondary lymphoedema, sivelestat.

INTRODUCTION

The lymphatic vasculature is critical for fluid homoeostasis, immune surveillance and fat absorption [1]. It comprises lymphatic capillaries, adapted for lymph uptake from the tissue interstitium, and collecting vessels, which transport lymph back to the vascular blood system. Lymphatic capillaries are blind-ending vessels, lined by a single thin layer of overlapping lymphatic endothelial cells (LECs) directly connected to the surrounding extracellular matrix (ECM) by means of elastic anchoring filaments (AFs) [2]. Abnormalities of AFs may reduce adsorption from the interstitium and propulsion of lymph and cells, and promote pathological conditions such as lymphoedema [3]. The secondary lymphoedema (acquired) frequently arises as a consequence of surgical, malignant, inflammatory or traumatic disruption of the lymphatics [4]. Lymphoedema has no cure and current treatments [5] can only slow its progression. The recent improvements in surgical and radiotherapy techniques have not substantially reduced the incidence of cancer-related lymphoedema and, although reliance on sentinel node techniques does reduce the risk of lymphoedema, only a small percentage of the at-risk cancer population benefits from this approach. Therefore, the impact of lymphoedema remains a serious healthcare problem in patients with cancer, above all in those with breast cancer.

Abbreviations: AF, anchoring filament; CI, cell index; ECM, extracellular matrix; H&E, haematoxylin and eosin; HMVEC–dLyNeo, human microvascular endothelial cell–dermal lymphatic – neonatal; Ig, immunoglobulin; LAEC, lymphangioma-derived endothelial cell; LEC, lymphatic endothelial cell; MMP, matrix metalloproteinase; NE, neutrophil elastase; TGF-β, tumour transforming factor β; VEGF, vascular endothelial growth factor; WT, wild type.

Correspondence: Paola Spessotto (email pspessotto@cro.it).

Lymphoedema, wound healing and tumour metastatic processes, in which lymphangiogenesis is a critical factor to initiate and coordinate the sequence of events, are closely related to the molecular ECM composition of the microenvironment. A better understanding of which and how ECM molecules influence endothelial cell functions could provide full insight into how lymphangiogenesis occurs and contributes to local lymph drainage in disordered tissues. The ECM protein EMILIN1 is expressed in lymphatic vessels, as well as in the connective tissues of a wide variety of organs [6–9]. EMILIN1 is a component of the system of cell anchorage to elastic lamellae via the $\alpha_4\beta_1$- and/or $\alpha_9\beta_1$-integrin receptors [10,11]. Although mice homozygous for disruption of *emilin1* display no lethal abnormalities [8,12,13], structural and functional defects of the lymphatic vessels are present, with a reduction in AFs, enlargement of lymphatic capillaries and alterations of the luminal valves of the collectors, with myofibrillar differentiation and proliferation [11].

There have been few attempts to develop suitable animal models of secondary lymphoedema and to assess new molecular therapies: the most recent are the mouse-tail skin wound [14,15] and the excision of mouse axillary lymph nodes [16]. The identification of several molecular components of the lymphatic vasculature has made it feasible to consider treatment with lymphatic growth factors. Vascular endothelial growth factor (VEGF)-C and VEGF-D have been tested in animal models, demonstrating that growth factor-induced maturation of lymphatic vessels is possible in adult mice and that growth factor therapy could become a valid approach for lymphoedema treatment [16–18]. Pharmacological approaches were also attempted; however, although ketoprofen reduced the swelling of the tail in a post-surgical mouse model [19,20], benzo-pyrones applied in human clinical trials were not very effective, apart from a slight improvement in lymphoedema [21,22].

We have recently demonstrated that neutrophil elastase (NE) was the most effective cleaving enzyme that could fully impair the regulatory function of EMILIN1 [23]. In the present study we demonstrate that, in the acute phase of lymphoedema, NE contributed to EMILIN1 degradation in the intercellular connections of LECs, altering their properties, and that the local administration of sivelestat, a specific NE inhibitor, reactivated lymphatic vessel function in a post-surgical tail lymphoedema model by reducing EMILIN1 cleavage.

MATERIALS AND METHODS

Reagents

Secreted recombinant EMILIN1 protein was obtained by constitutive expression in 293E cells, as previously described [24]. Briefly, the cells were expanded to mass culture and then maintained for 2 days in serum-free medium to allow accumulation of EMILIN1 in the cell supernatant. Partial purification was achieved by dialysis of the conditioned medium at 4 °C against 0.1 M NaCl, 20 mM Tris/HCl, pH 6.8. A further purification step was achieved by chromatography on a DEAE-cellulose column and size exclusion chromatography using Sepharose CL 4B (1.0×90.0 cm column, Amersham Pharmacia Biotech). Fibronectin was purchased from Sigma-Aldrich.

NE was purchased from Calbiochem (324681, Merk Millipore) and MMP-14 from Giotto Biotech S.r.l. Sivelestat sodium salt hydrate was purchased from Sigma (S7198) and suspended in a 20 mg/ml stock solution. GM6001 (Chemicon, Merk Millipore) was used as a broad-spectrum matrix metalloproteinase (MMP) inhibitor.

A complete list of all antibodies used in this study, with their specificity and sources/manufacturers, is given in Supplementary Table S1.

Mouse-tail model of lymphoedema

All animal procedures and their care were performed according to the institutional guidelines, in compliance with national laws and authorization by the Italian Ministry of Health (no. 248/2015). C57Bl/6 mice were purchased from Charles River Laboratories. *Emilin1*$^{-/-}$ mice (C57Bl/6 background) were generated as previously described [13] and maintained at the CRO-IRCCS mouse facility. In all experiments 6- to 8-week-old female animals and their littermate age-matched controls were used. Mice were anaesthetized with an intraperitoneal injection of ketamine (Imalgene, Merial) (100 mg/kg) and xylazine (Rompun, Bayer) (10 mg/kg). To provide analgesia for the treatment of post-surgical pain, a buprenorphine (Temgesic solution, 0.3 mg/ml, RB Pharmaceutical Ltd) subcutaneous injection was performed before surgery. To induce lymphoedema, a circumferential incision was made through the dermis close to the tail base (1 cm) to sever the dermal lymphatic vessels. The edges of this incision were then pushed apart with a cauterizing iron, thereby disturbing the deeper lymphatics, preventing superficial bleeding and creating a 2- to 3-mm gap to delay wound closure. Care was taken to maintain the integrity of the major underlying blood vessels and tendons so that the tail distal to the incision did not become necrotic. Gentamicin sulfate 0.1 % ointment (Gentalyn, MSD Italia S.r.l.) was applied to prevent infection. To counteract NE, sivelestat solution (2 mg/kg, final concentration) was intradermically injected with a 29-gauge syringe, immediately after surgery and daily for the following 4 days. Pilot dose–response experiments (three mice per group) were carried out to find the optimal inhibitor concentration. Volumetric assessment was performed by taking a picture of the tail close to a ruler [25]. On acquired images, computer-assisted morphometric analyses were performed using ImageJ software (accessible at http://imagej.nih.gov/ij/). The tail volume was calculated with the truncated cone formula and the tail-volume increase for each mouse was calculated on the basis of presurgical measurements.

Mice were sacrificed at various times up to 14 days from surgery. The tails were excised proximally and distally from the site of the wound. Tail tissues were fixed in 10 % formalin-buffered solution, and decalcified with EDTA before OCT medium embedding (Kaltek). Cross-cryostat sections of 5 μm were prepared and stored at −80 °C until processing.

To test the enzymatic activity of lymph derived from mice subjected to tail surgery, mice were sacrificed at days 4 and 7. Oedematous tail tissue was excised and removed close to the site of wound and immediately centrifuged at 4 °C in a

microcentrifuge at maximum speed for 30 min. The supernatant was collected and stored at −80 °C until its use for *in vitro* experiments.

In vivo administration of anti-Ly6G antibody to deplete neutrophils

Mice were injected intraperitoneally with 500 μg of anti-Ly6G antibody (clone 1A8, BioXCell) dissolved in 200 μl of PBS, the day before tail surgery and daily for the following days. Control mice received equal amounts of isotope control antibodies (rat immunoglobulin IgG2a, clone 2A3, BioXcell). Flow cytometry was performed to check depletion of neutrophils by anti-Ly6G treatment as follows: blood samples were collected in tubes containing EDTA and treated with ammonium chloride erythrocyte lysis buffer; cells were stained directly with conjugated antibodies (see Supplementary Table S1) for 15 min at 4 °C in the dark in PBS/1 % BSA. The Gr1 antibody was used here to avoid false-negative results because the anti-Ly6G-depleting antibody may mask the Ly6G epitope. All analyses were performed using a Beckton Dickinson LSRII flow cytometer using dedicated Diva software.

Cell cultures

Human microvascular endothelial cell–dermal lymphatic – neonatal (HMVEC–dLyNeo) cells, and the media optimized for their growth (EBM-2), were purchased from Lonza (Euroclone SpA). These cells have been characterized as previously described [8] and reported in Supplementary Figure S1. Mouse lymphangioma-derived endothelial cells (LAECs) were isolated and immortalized following the procedure described previously [26]. Briefly, the mice were injected twice intraperitoneally, with a 15-day interval, with 200 μl of emulsified (1:1 with PBS) incomplete Freund's adjuvant (Sigma). Hyperplastic vessels were isolated from the liver and diaphragm at day 30 and treated with 0.5 mg/ml of collagenase A (Roche Diagnostics), and the resulting single-cell suspension was cultured. After 7–10 days of culture, subconfluent cells (LAECs) were recovered with trypsin/EDTA and immortalized by means of SV40 infection. Immortalized LAECs were characterized for lymphatic endothelial markers as reported previously by us [27].

Human samples

To analyse EMILIN1 degradation in human lymphoedematous tissues, samples were obtained after signed informed consent from patients affected by peripheral secondary lymphoedema who underwent lymphatic microsurgery at the Centre of Lymphatic Surgery and Microsurgery of the University of Genoa, Italy. During derivative procedures of multiple lymphatic–venous anastomoses or lymphatic pathway reconstruction [28], surgeons sectioned small tissue samples for *in vitro* analyses. To quantify inflammatory infiltrate we retrieved biopsy material from two patients with lymphoedema of the vulva, which developed after adjuvant radiotherapy for cervical cancer and was at a later stage treated for lymphoedema resolution at CRO-IRCCS, as recently reported [29]. For histological analysis, formalin-fixed, paraffin-embedded, 5-μm tissue sections were deparaffinized in xylene and rehydrated in a graded series of alcohol. Images of haematoxylin and eosin (H&E)-stained paraffin sections were captured using a camera (ICC50, Leica Microsystems) connected to a Leica DM 750 microscope.

Immunofluorescence and histological analyses

For immunofluorescence staining, cells were washed and fixed with 4 % paraformaldehyde for 10 min, permeabilized (with 1 % BSA, 0.1 % Triton X-100 and 2 % FBS in PBS) for 5 min and saturated with the blocking buffer (1 % BSA, 2 % FBS in PBS) for 30 min. Tail-tissue sections were hydrated for 15 min (with 1 % Triton X-100, in PBS) and blocked for 30 min (1 % BSA, 2 % FBS or 5 % normal goat serum in PBS). For HMVEC–dLyNeo cell staining, rabbit polyclonal anti-human EMILIN1 antibodies (As556, produced in our laboratories), mouse monoclonal anti-human CD31 antibodies and rabbit polyclonal anti-human fibronectin antibodies (a gift of Professor GM Bressan, University of Padua, Italy) were used. For tail-tissue cryostat sections rat monoclonal anti-mouse EMILIN1 antibodies (clone 1007C11A8, produced in our laboratories) and hamster anti-mouse podoplanin antibodies were used. All the incubations with the primary antibodies were performed overnight at 4 °C (followed by three 5-min washes in PBS) and with the appropriate secondary antibodies (conjugated with Alexa Fluor 488 or Alexa Fluor 546 at 1:200 dilution, Life Technologies) for an additional 1 h at room temperature. For all samples, negative controls included the corresponding isotype or IgG. To-Pro-3 (1:5000, Life Technologies) was used to visualize the nuclei. Images were acquired with a true confocal scanner system (TCS SP2, Leica Microsystems) equipped with HC PL Fluotar 10×/0.30 NA, HCX PL Apo 40×/1.25–0.75 NA and HCX PL Apo 63×/1.40–0.60 NA oil objectives (Leica), using Leica confocal software.

Cryostat sections were stained with H&E and images were acquired using an optical microscope (Leica DM750) equipped with a CCD camera using dedicated software (Las EZ Leica).

Western blot analysis

Mice were sacrificed at day 4 or 7 after surgery, and lymph samples were collected from tails and incubated with recombinant EMILIN1 for 18 h. Whole lysates of both human samples and tail tissues from normal and lymphoedematous sites were prepared using thiourea/urea lysis buffer (7 M urea, 2 M thiourea, 2 % CHAPS). Samples were subjected to SDS/4–12%PAGE (using Criterion Precast Gel, BioRad) and blotted on nitrocellulose membranes (Amersham Hybond-ECL, Amersham Pharmacia Biotech). Membranes were blocked (5 % non-fat milk, 0.1 % Tween-20 in TBS) and incubated with rabbit polyclonal anti-human EMILIN1 (As556) to identify recombinant human EMILIN1 protein or rabbit anti-mouse EMILIN1 (mC1q, an antibody generated to specifically recognize the mouse gC1q domain) to detect EMILIN1 in mouse tissue lysates. Horseradish peroxidase (HRP)-tagged secondary antibodies (Jackson Immunoresearch) were used at proper dilutions. Signals were detected using ECL reagents (Amersham Western Blotting Detection System and HyperFilm ECL, Amersham Pharmacia Biotech).

Microlymphangiography

Mice were anaesthetized as described above and the functionality of tail lymphatics was examined by fluorescence

microlymphangiography; 2 μl of 5 mg/ml FITC–dextran solution (M_r ~2000 kDa, Life Technologies) was injected near the surgical wound (0.5 cm distant) and diffusion of the dye was immediately recorded using a stereomicroscope Leica M205 FA and Leica DFC310 FX digital camera (Leica Microsystems). After 5 min, mice were sacrificed and draining iliac lymph nodes were imaged as above.

Endothelial barrier integrity assays

To measure endothelial barrier integrity we adopted the technology provided by the Real-Time Cell Analyzer dual plate instrument (ACEA Biosciences) and proprietary E-plates 96 [30,31]. The principle of this technology relies on the fact that the increase in electrode impedance, expressed as the cell index (CI), is directly dependent on the number of cells and their spread. Thus, the CI is a reflection of overall cell number, attachment quality and cell morphology which can change as a function of time. HMVEC-dLyNeo or LAEC cells (5×10^3/well) were added to E-plates 96 in EBM-2 medium. After 4 days, different concentrations of NE were added and the E-plates 96 were monitored every 15 min for 12 h. Changes in impedance of confluent endothelial cells reflect changes in barrier function. Data analysis was performed using the Real-Time Cell Analyzer software (version 1.2) supplied with the instrument. Experiments were performed in triplicate and data are expressed as a normalized CI at the time of NE addition.

Statistical analysis

Throughout this study, plotted values are shown as means$\pm$S.E.M.s or S.D.s as indicated. The statistical significance of the results was determined using the two-tailed unpaired Student's *t*-test to determine whether the two datasets were significantly different. A value of $P < 0.05$ was considered significant.

RESULTS

Lymphatic function is reduced in *Emilin1*$^{-/-}$ mice

Using a post-surgical tail lymphoedema approach we demonstrate that *Emilin1*$^{-/-}$ mice show a faster, greater and much longer persistence of swelling compared with the wild-type (WT) littermates (Figures 1A and 1B), suggesting that the absence of EMILIN1 correlates with the inefficient fluid drainage by the lymphatics. No significant differences in the number of lymphatic vessels were detected, 2 weeks after surgery, in the proximal segment of the wound between WT and *Emilin1*$^{-/-}$ mice, whereas, in the distal oedematous tail tissues, very few lymphatic capillaries were present in *Emilin1*$^{-/-}$ mice (Figures 1C and 1D). Moreover, new lymphatic vessels of WT mice had a larger lumen compared with *Emilin1*$^{-/-}$ mice (Figures 1C and 1E). To analyse lymphatic regeneration and function in WT and *Emilin1*$^{-/-}$ animals further, we performed lymphangiography to visualize draining lymph nodes. After the injection of FITC–dextran in the dermis of distal lymphoedematous tails, the typical hexagonal network of dermal lymphatics driving the fluorescent tracer was detectable in WT but not *Emilin1*$^{-/-}$ mice (Figure 2A). Consequently, only WT mice were able to drain FITC–dextran to iliac lymph nodes (Figure 2B). In fact, the uptake of FITC–dextran by lymphatic vessels was easy to detect in both the proximal and the distal tail segments in WT mice, indicating that the regeneration of lymphatics after surgery had occurred successfully (Figure 2C). On the other hand, the fluorescent dye persisted in the dermis of *Emilin1*$^{-/-}$ mice and no close association of FITC–dextran with lymphatic vessels was evident (Figure 2C). The lack of a well-defined capillary network in the distal tail and the absence of fluorescent dye in draining lymph nodes in *Emilin1*$^{-/-}$ animals suggested that EMILIN1 deficiency impaired the regeneration of functional lymphatic vessels.

Neutrophils infiltrate the lymphoedematous tissues

The surgical approach entails an acute inflammatory response with the release of proteolytic enzymes. Neutrophils represented the prevalent inflammatory cells of the infiltrate 4 days after surgery (Figure 3A; see also Figure 7). EMILIN1 was digested to a 120-kDa form after *in vitro* incubation with the lymph extracted from post-surgical lymphoedema tissues (Figure 3B). The enzymatic activity in the lymph persisted up to day 7 after surgery in both WT and *Emilin1*$^{-/-}$ mice. This molecular degradation form is reminiscent of that obtained after NE treatment of purified EMILIN1 [23]. This cleavage effect was abolished with the addition of sivelestat, a well-known NE inhibitor [32–34], but not with GM6001, a broad-spectrum MMP inhibitor, indicating that, among the enzymes released by neutrophils, NE was the most, if not even the only one, effective in EMILIN1 fragmentation (Figure 3C). Consequently, only sivelestat could inhibit the activity of NE on recombinant EMILIN1 *in vitro* (Figure 3D). Furthermore, in contrast to normal skin, in lymphoedematous WT tissues the intact form of EMILIN1 was not detectable, whereas a major EMILIN1 fragment of about 70 kDa was generated (Figure 3E), showing that EMILIN1 digestion occurred after a surgical wound in the tail.

EMILIN1 degradation and neutrophil infiltration in human acquired lymphoedema

Samples derived from surgical specimens of peripheral secondary lymphoedema, obtained during lymphatic microsurgery, were assayed using Western blots to determine EMILIN1 expression levels. All samples expressed different amounts of intact as well as fragmented EMILIN1 (Figure 4A). Variable amounts of the most characteristic bands detected in the NE-derived fragmentation pattern were present (Figure 4A, black arrows), suggesting that in human lymphoedematous samples EMILIN1 was also digested by NE. The source of NE is probably due to the presence of neutrophils, as detected in human acquired lymphoedema of the vulva, which developed in two patients affected by cervical cancer and treated with adjuvant radiotherapy (Figure 4B). Even if these latter samples have to be considered part of a chronic inflammatory process, as demonstrated by the presence of several macrophages (CD68-positive cells) and a few lymphocytes (CD3- and CD20-positive cells) (see Supplementary Figure S2), neutrophils were detected nearby or even attached to LECs (Figure 4B).

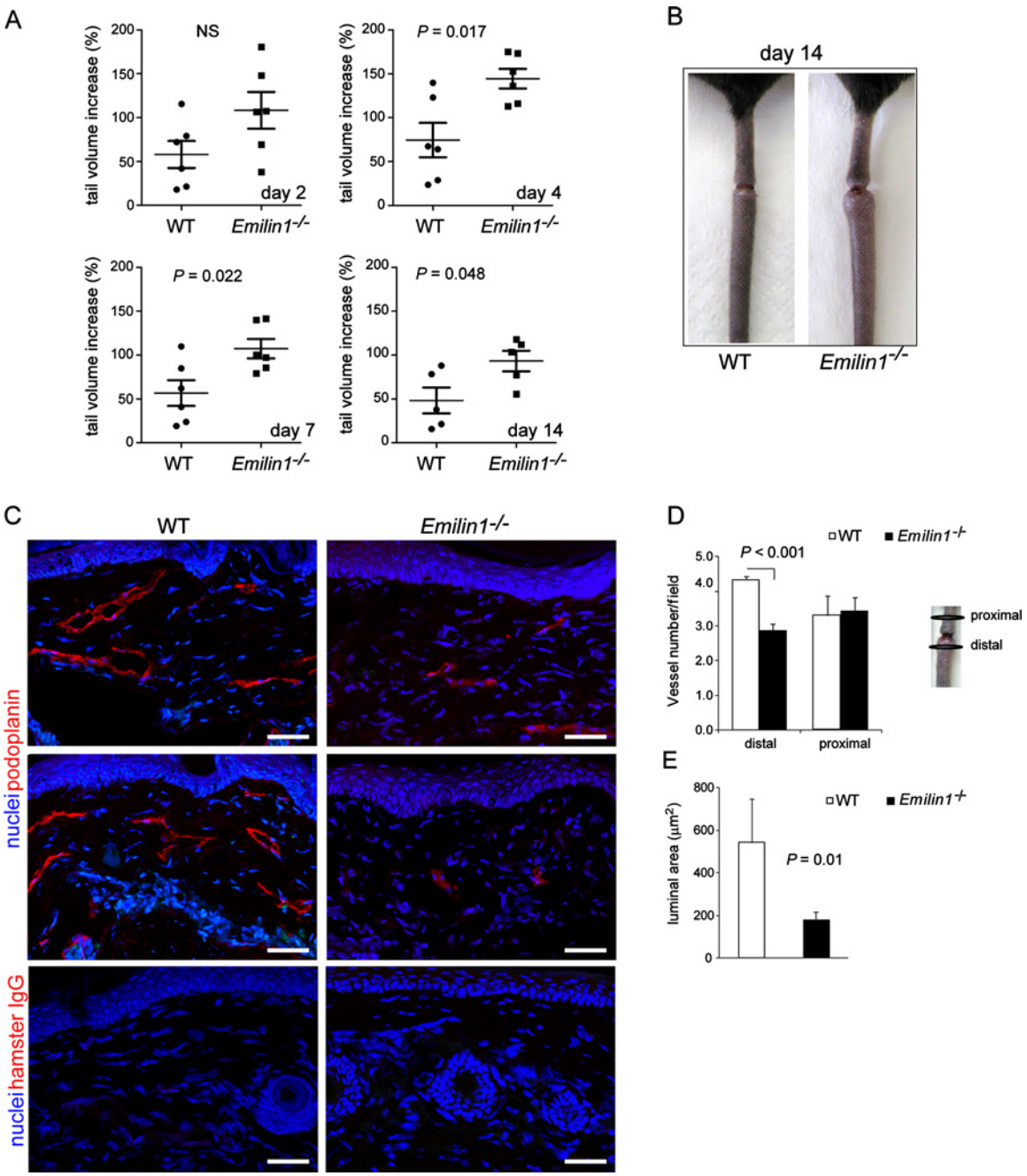

Figure 1 ***Emilin1*$^{-/-}$ mice develop consistent lymphoedema after tail surgery**

(**A**, **B**) *Emilin1*$^{-/-}$ mice showed a greater and much longer persistence of swelling compared with their WT littermates; six mice per group were used. NS, not significant. (**C**) Representative cryostat sections from two WT (left) and two *Emilin1*$^{-/-}$ (right) mice of the distal part of their tail, demonstrating that the number of podoplanin-positive lymphatic vessels was higher in WT than in *Emilin1*$^{-/-}$ mice. Isotypical control staining was included. (**D**) Quantitative analyses of vessel density (podoplanin staining) in proximal and distal parts of the tail. The number of podoplanin-positive lymphatic vessels was counted in the whole immunofluorescent section acquired by the Leica TCS SP2 confocal system, using Volocity software provided by Perkin Elmer. (**E**) In distal tails, new lymphatic vessels of WT mice have a larger lumen compared with *Emilin1*$^{-/-}$ mice. The luminal area was calculated using the measurement area tool of Volocity software. The graphs report the means$\pm$S.E.M.s obtained from four mice per group, analysing eight fields for each sample. Scale bar = 50 μm.

NE degrades EMILIN1, impairing lymphatic endothelium integrity

To demonstrate that EMILIN1 cleavage directly altered LEC properties, we analysed the integrity of the monolayer by monitoring the impedance of confluent endothelial cells after NE treatment. The addition of NE resulted in a dose-dependent effect on the barrier function permeability (Figures 5A and 5B) without affecting cell viability (data not shown), indicating that this

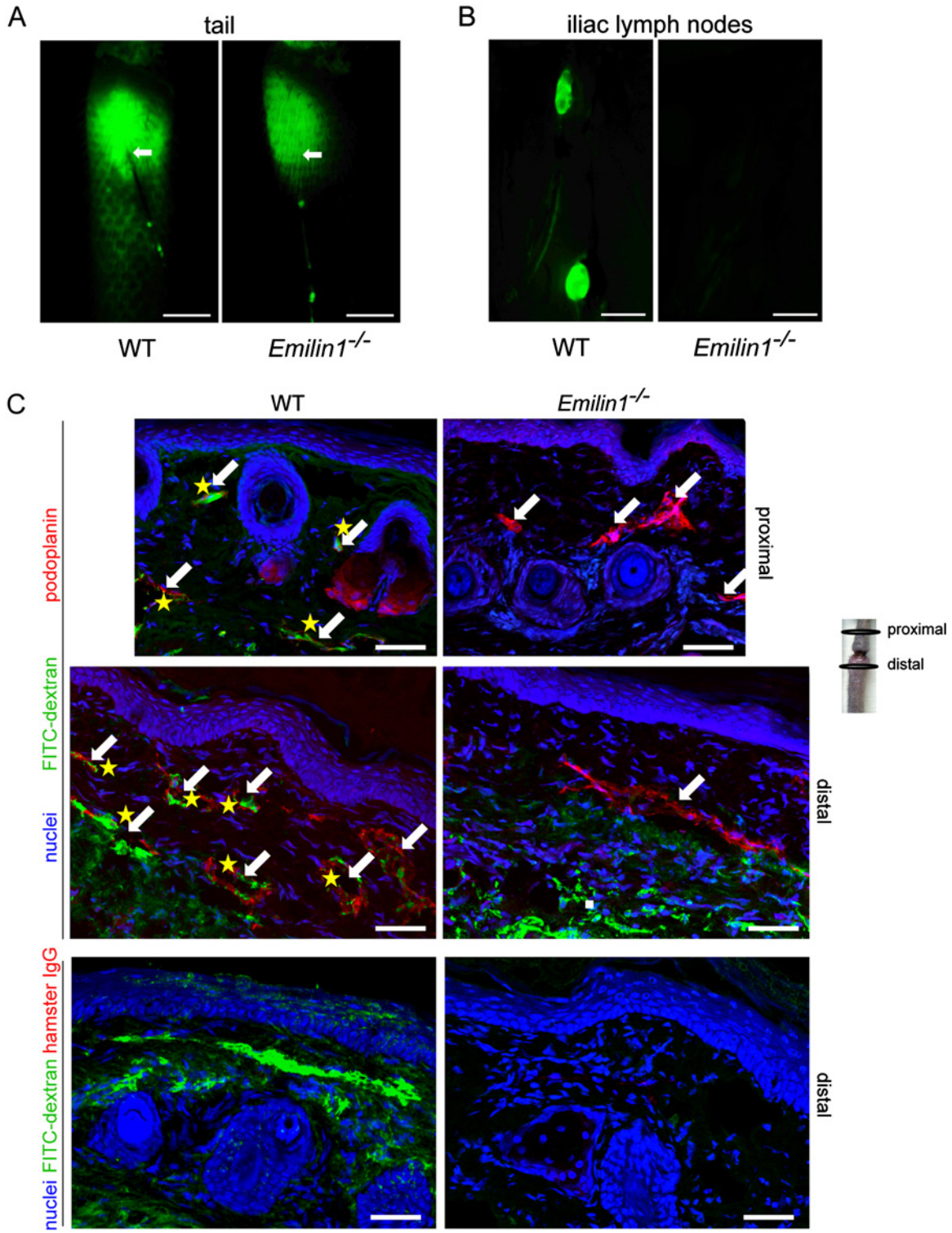

Figure 2 **Reduced lymphatic function in *Emilin1*$^{-/-}$ mice after tail surgery**

FITC–dextran was subcutaneously injected into the tail of WT and *Emilin1*$^{-/-}$ mice at day 14 after wounding. (**A**) Representative fluorescence images of subcutaneous lymphatic vessels in the tail are shown: note the typical hexagonal network in WT tails. White arrows indicate the FITC–dextran injection site. (**B**) At 5 min from injection, images were taken to visualize draining iliac lymph nodes. (**C**) Tails were harvested and stained with anti-podoplanin antibodies. Note the uptake of FITC–dextran by lymphatic vessels (yellow asterisks) in WT mice and the persistence of the dye in the dermis in *Emilin1*$^{-/-}$ mice. White arrows indicate podoplanin-positive lymphatic vessels. Isotypical control staining was included. Scale bars = 2 mm (A, B) and 50 μm (C).

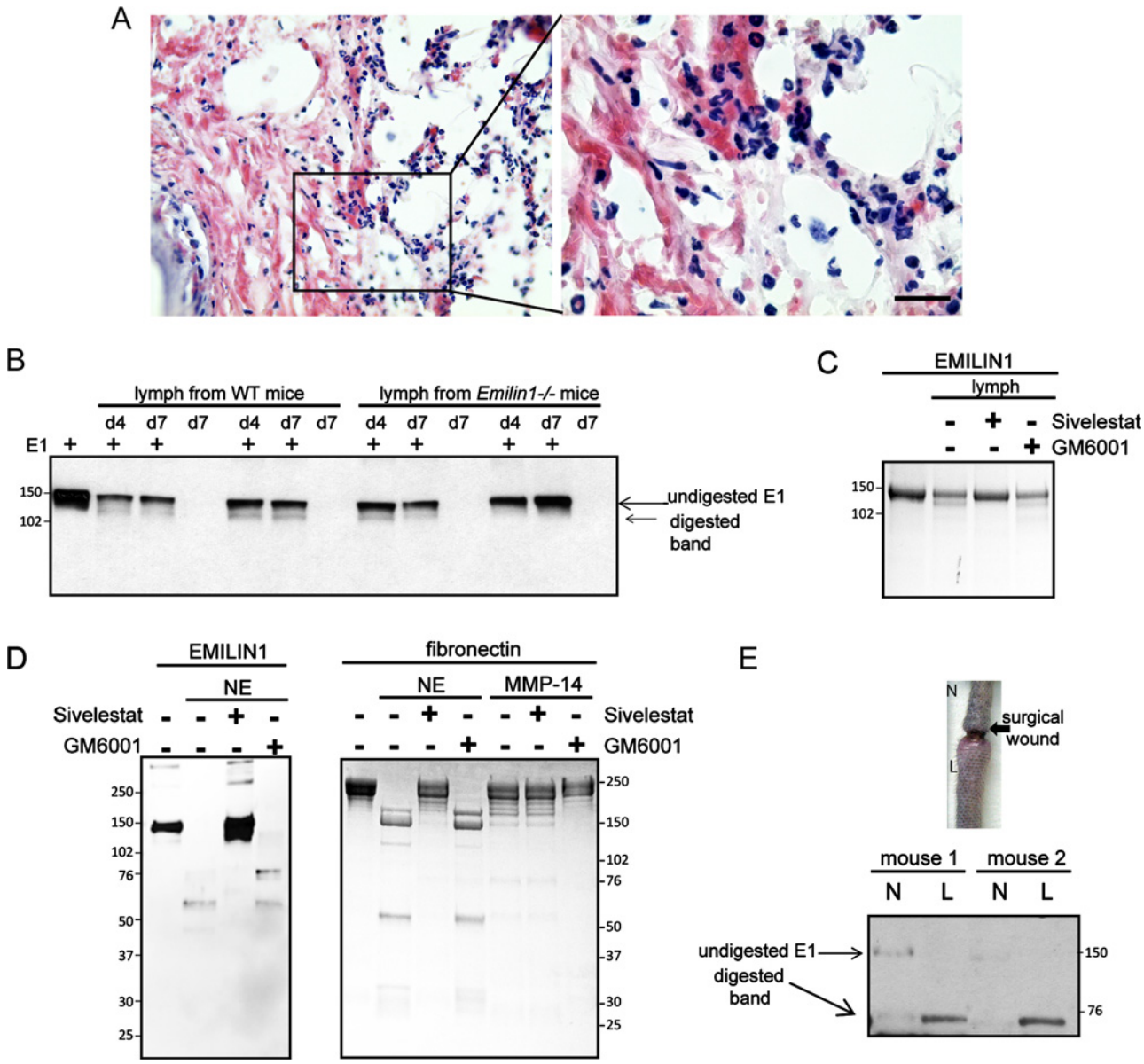

Figure 3 **Neutrophil infiltration after tail surgery is associated with EMILIN1 cleavage**

(**A**) Representative H&E staining of cryostat tail section (left) and its boxed area magnification (right) at day 4 after surgery, showing an abundant neutrophil infiltrate. (**B**) Western blot analysis of recombinant EMILIN1 (E1) fragmentation *in vitro* after an 18-h incubation with the lymph extracted from WT and *Emilin1*$^{-/-}$ mice at day 4 (d4) or 7 (d7) after wounding. (**C**) Sivelestat, but not GM6001, blocked the enzymatic activity of the lymph on recombinant EMILIN1. (**D**) Coomassie Blue-stained gels show that recombinant EMILIN1 cleavage using NE was specifically blocked by sivelestat. Fibronectin was used as positive control for MMP-14 and the MMP inhibitor GM6001. (**E**) Western blot analysis of EMILIN1 degradation in normal (N) and lymphoedematous (L) tail tissue extracts. Scale bar = 20 μm.

enzyme treatment could loosen cell junctions as demonstrated by CD31 distribution (Figures 5C–5F). After NE treatment, cells appeared smaller with looser intercellular junctions, and EMILIN1-positive fibrils were not evident in the gaps between cells, suggesting that its cleavage correlated with the markedly reduced cellular contacts (Figure 5D). Fibronectin staining seemed to be unmodified intercellularly after NE treatment (Figures 5E and 5F), probably because the elected substrate for NE in this context was EMILIN1 and the integrity of EMILIN1 determined the stability of the LEC junctions. CD31 staining was clearly visible and intense in cellular protrusions after NE treatment, indicating that the NE-dependent formation of intercellular gaps was probably attributed to ECM degradation rather than to proteolysis of membrane receptors (Figure 5D). Accordingly, LECs obtained from *Emilin1*$^{-/-}$ mice were not affected by NE treatment (Figure 5B), suggesting that NE's effects on LEC integrity were exerted by affecting primarily EMILIN1.

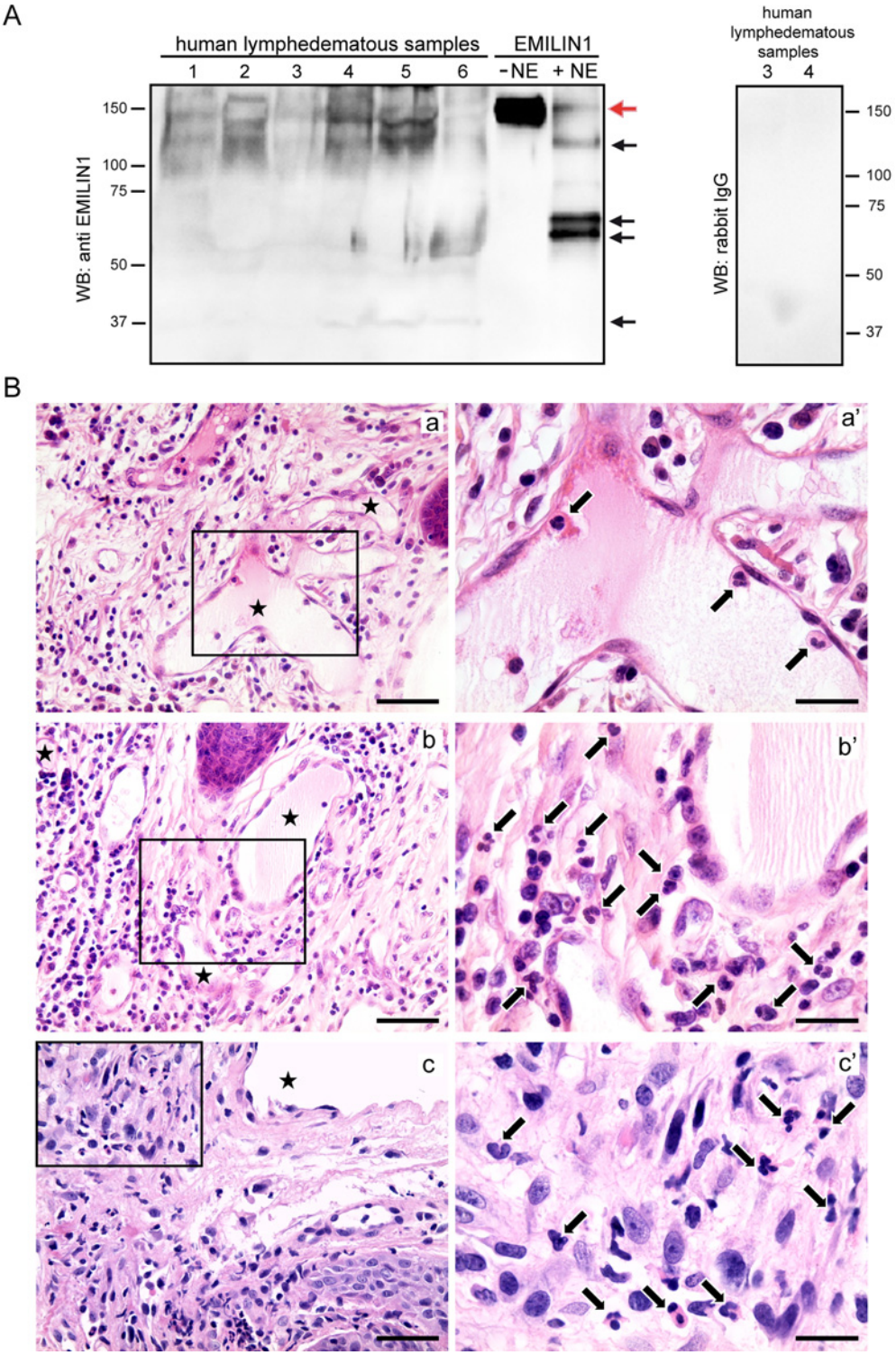

Figure 4 **EMILIN1 cleavage and neutrophil infiltration in human acquired lymphoedema**

(**A**) Western blotting analysis of EMILIN1 expression and cleavage in human acquired lymphoedema samples. Black arrows and red arrow indicate the most representative bands of cleaved EMILIN1 and undigested EMILIN1, respectively. (**B**) Paraffin-embedded sections of vulvar lymphoedema samples obtained from two patients (a and b, patient no. 1; c, patient no. 2) stained with H&E. Arrows indicate neutrophils (a′, b′, c′) and asterisks enlarged lymphatic vessels (a, b, c); a′, b′ and c′ correspond to the boxed areas in a, b and c, respectively. Scale bars = 20 μm (a′, b′, c′); 50 μm (a, b, c).

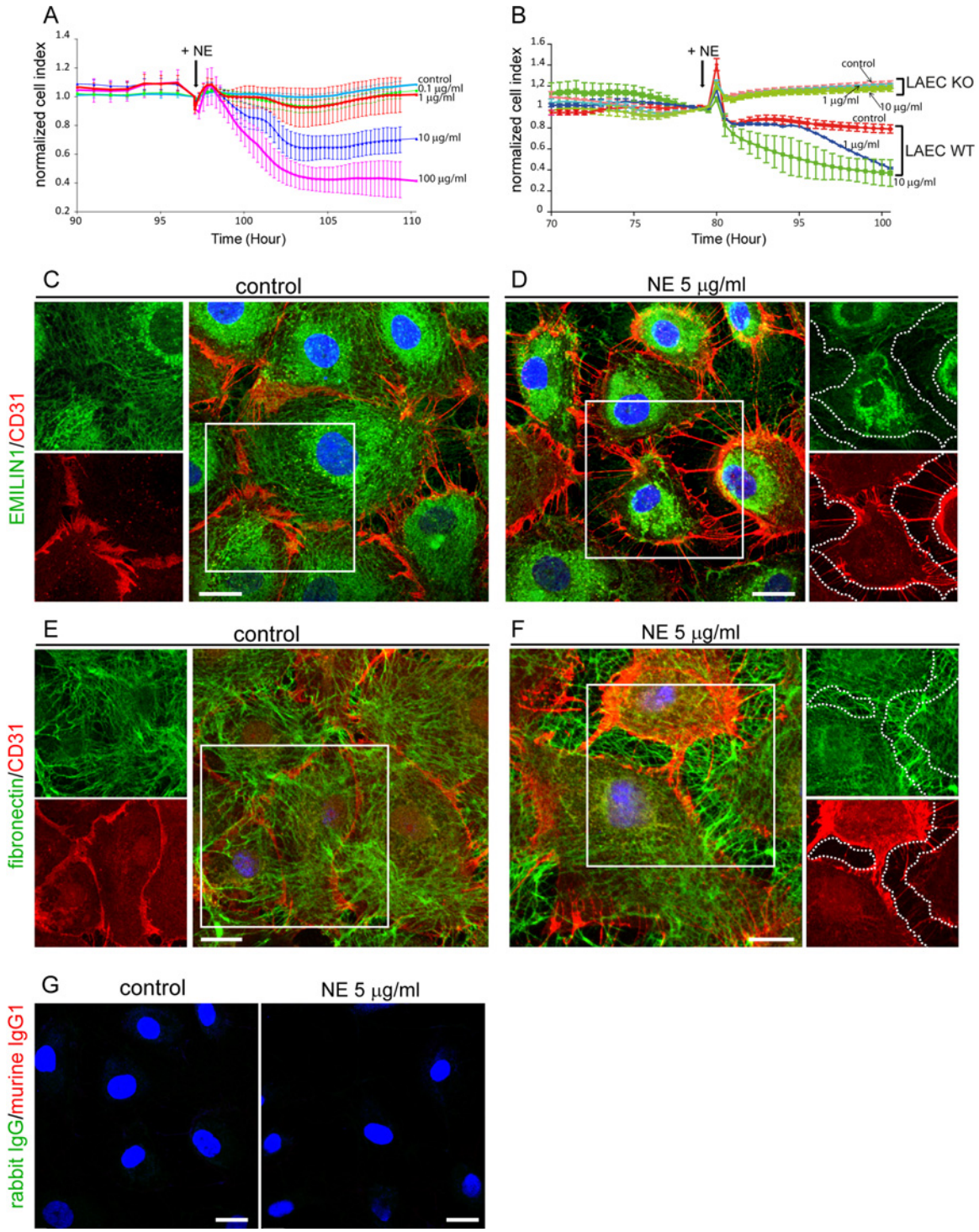

Figure 5 **EMILIN1 degradation by NE impairs lymphatic endothelium integrity**

(**A**, **B**) Dynamic monitoring of lymphatic endothelium integrity in response to NE measured with XCelligence instrument and expressed as normalized CI. Cells were grown to confluence and then (black arrows in the graphs) different doses of NE were added. HMVEC (A) and mouse LECs from WT (LAEC WT) and *Emilin1*$^{-/-}$ (LAEC KO) mice (B) were used. The means$\pm$S.D.s of three independent experiments are reported in the graphs. (**C**–**F**) Confluent HMVECs were incubated for 5 h with NE and then fixed and stained with anti-CD31 and anti-EMILIN1 (C, D) or anti-fibronectin (E, F) antibodies. Dotted lines highlight loss of EMILIN1 (D) or the well-detected and distributed fibres of fibronectin (F) within the area separating adjacent cells after NE treatment. (**G**) Isotypical control staining of confluent HMVECs. Scale bar = 20 μm.

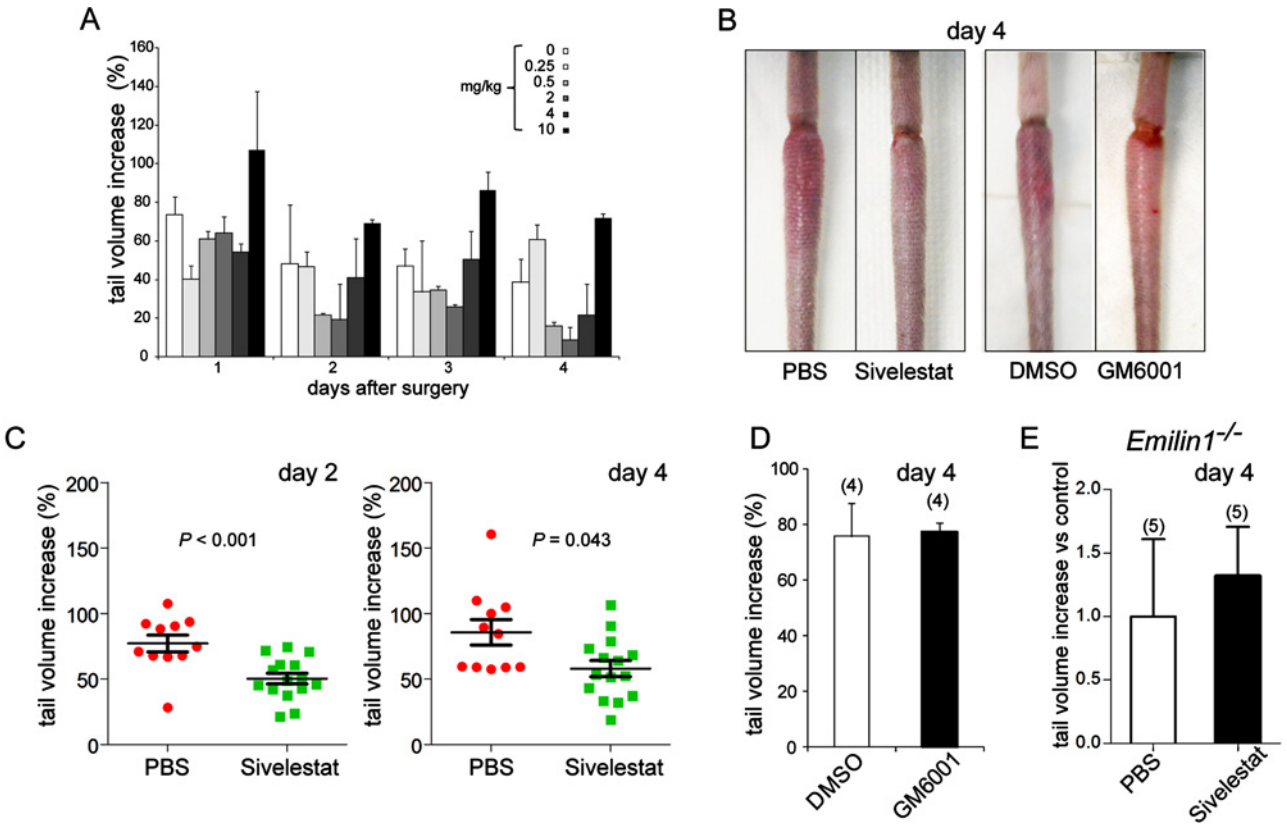

Figure 6 **Sivelestat specifically reduces tissue swelling in a post-surgically induced lymphoedema model**
(**A**) Dose–response effect of sivelestat on tail-volume increase after induction of surgical lymphoedema. Three mice per group were subjected to local treatment. PBS (indicated as '0 mg/kg') was used as control 'treatment'. (**B**–**D**) Sivelestat, but not GM6001, already significantly reduced the extent of swelling in WT mice from the first days after injury. The vehicle DMSO was used as a control for GM6001. (**E**) Sivelestat had no effect when locally injected in *Emilin1*$^{-/-}$ mice. The numbers of mice used in (D) and (E) are reported in parentheses. Data are expressed as means±S.E.M.s.

Treatment with NE inhibitor reduces lymphoedema

We hypothesized that local treatment with NE inhibitors, by preventing EMILIN1 degradation, could reduce the extent of lymphoedema in WT mice. Immediately before wound surgery and daily for the next 4 days, WT animals were treated with sivelestat, which displays powerful treatment effects in various preclinical models [35]. We observed that, right from the early days after surgery, sivelestat-treated mice developed a significantly ($P < 0.001$) less intense swelling of the distal tail compared with the control (PBS-treated) mice (Figures 6A–6C, 7A and 7B). On the contrary, the local administration of GM6001 (5 mg/kg, following the same schedule used for sivelestat treatment) was unsuccessful in reducing lymphoedema (Figures 6B and 6D), indicating that MMPs were not responsible for the pathogenesis of lymphoedema. The possibility that EMILIN1 was the crucial target of NE in the acute phase of lymphoedema was strongly suggested by the results in *Emilin1*$^{-/-}$ mice, in which sivelestat had no effect in reducing tail swelling (Figure 6E).

The role of neutrophils in the tail lymphoedema model

Sivelestat did not inhibit the recruitment of neutrophils, which could also be detected up to day 7 after surgery in the tail dermis, as well as in PBS-treated mice (Figures 7C and 7D). The numbers of CD45- and CD68-positive cells did not significantly change after sivelestat administration (Figures 7E and 7F), indicating that this synthetic inhibitor specifically acted primarily on the enzymatic NE activity, and was ineffective on inflammatory cell recruitment. Sivelestat was also not influential in *Emilin1*$^{-/-}$ mice, which, however, had higher basal numbers of macrophages compared with WT mice (Figure 7E).

As neutrophils are the principal source of NE, we reasoned that neutrophil depletion could provide the same effect as obtained by sivelestat. We successfully depleted neutrophils by daily *in vivo* administration of anti-Ly6G monoclonal antibody (Figures 8A–8C). Accordingly, the number of CD45+ cells was dramatically reduced (Figure 8C). No significant change in the number of CD68+ cells was detected (Figure 8D). Two consequences of the cell depletion were the reduction in the extent of tail swelling 4 days after surgery (Figure 8F) and a higher EMILIN1 staining compared with control mice (Figure 8E). The effects of Ly6G treatment suggest that EMILIN1 fragmentation was reduced, but not sufficiently to prevent the loss of its integrity and obtain a significant reduction in swelling, as occurred after sivelestat treatment. In fact, NE was still detectable in Ly6G-treated

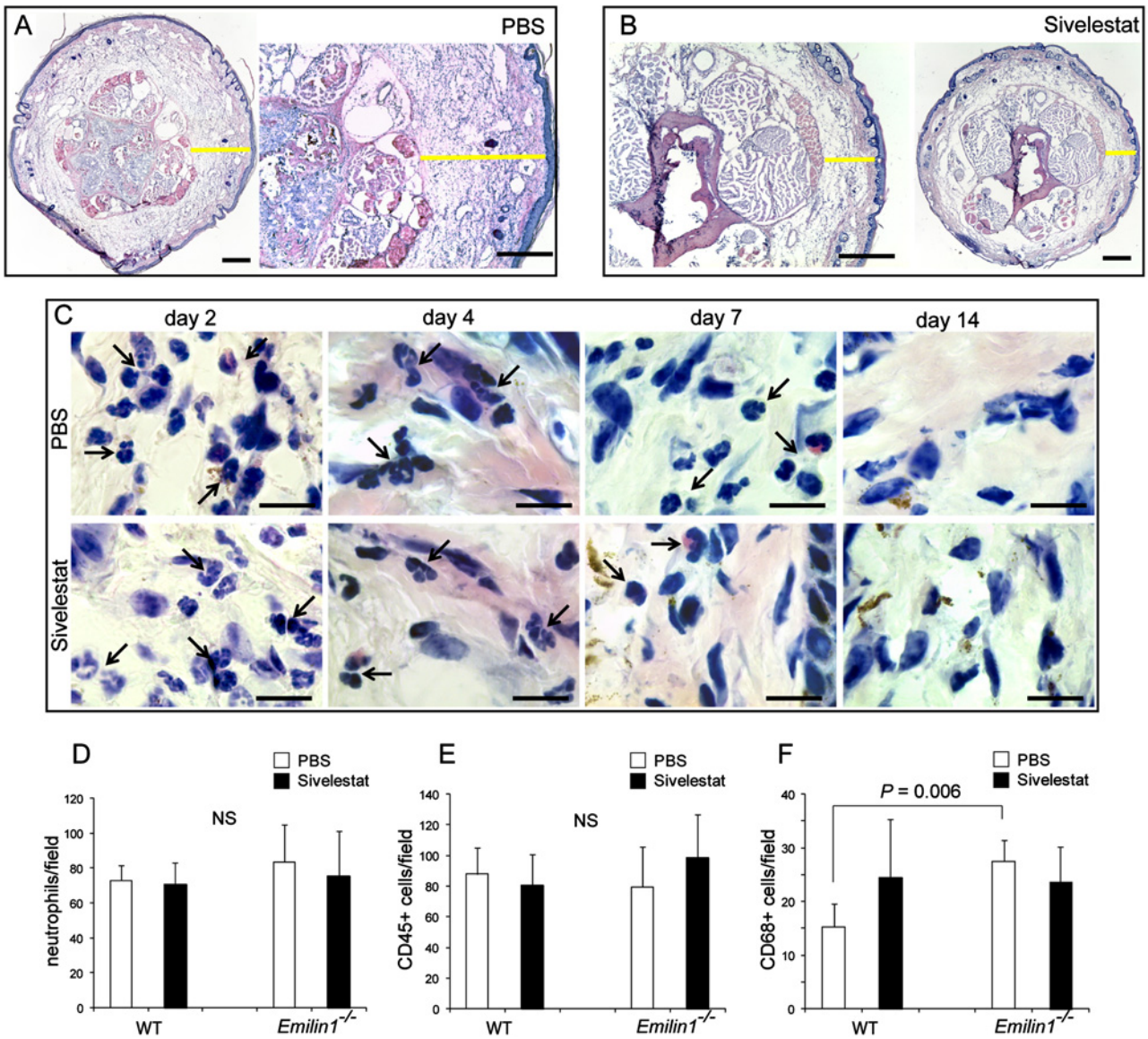

Figure 7 **Sivelestat does not interfere with neutrophil recruitment**

(**A**, **B**) Yellow lines in representative cryostat sections after H&E staining indicate the dermis thickness of the tail 4 days after surgery in (A) control (PBS) and (B) sivelestat-treated mice. (**C**) High magnification images of the tail dermis show the presence of an abundant neutrophil infiltrate at days 2 and 4 in both control and treated mice, demonstrating that sivelestat administration does not inhibit the recruitment of neutrophils, which are also detectable up to day 7 after surgery. Black arrows indicate neutrophils. (**D**–**F**) Quantitative analyses of the number of (D) neutrophils, (E) CD45- and (F) CD68-positive cells in the tail 4 days after surgery in control (PBS) and sivelestat-treated WT and *Emilin1*$^{-/-}$ mice. The graphs report the means$\pm$S.D.s obtained from four mice per group, analysing eight fields (40×, original magnification) for each sample. The number of neutrophils was calculated on H&E-stained sections on the basis of morphological criteria, whereas the number of CD45- and CD68-positive cells was calculated on immunofluorescent sections. Scale bars = 500 μm (A, B) and 20 μm (C).

mice even if the number of neutrophils was dramatically reduced (Figures 8B and 8E).

Local inhibition of EMILIN1 degradation reactivates lymphatic functionality

In time-course treatment experiments, EMILIN1 staining was clearly and highly reduced in control animals: EMILIN1, completely absent in organized fibrils at day 2 after surgery, became evident at day 7 and then it became associated with podoplanin-positive vessels only at day 14 (Figure 9A). A well-organized EMILIN1 matrix, albeit at a lower expression at day 2, could be detected in sivelestat-treated mice, and EMILIN1 was very closely associated with lymphatic cell membranes at all time points examined (Figures 9A and 9B). More interestingly, NE inhibition was already sufficient to restore lymphatic functionality after 4 days in WT mice: FITC–dextran

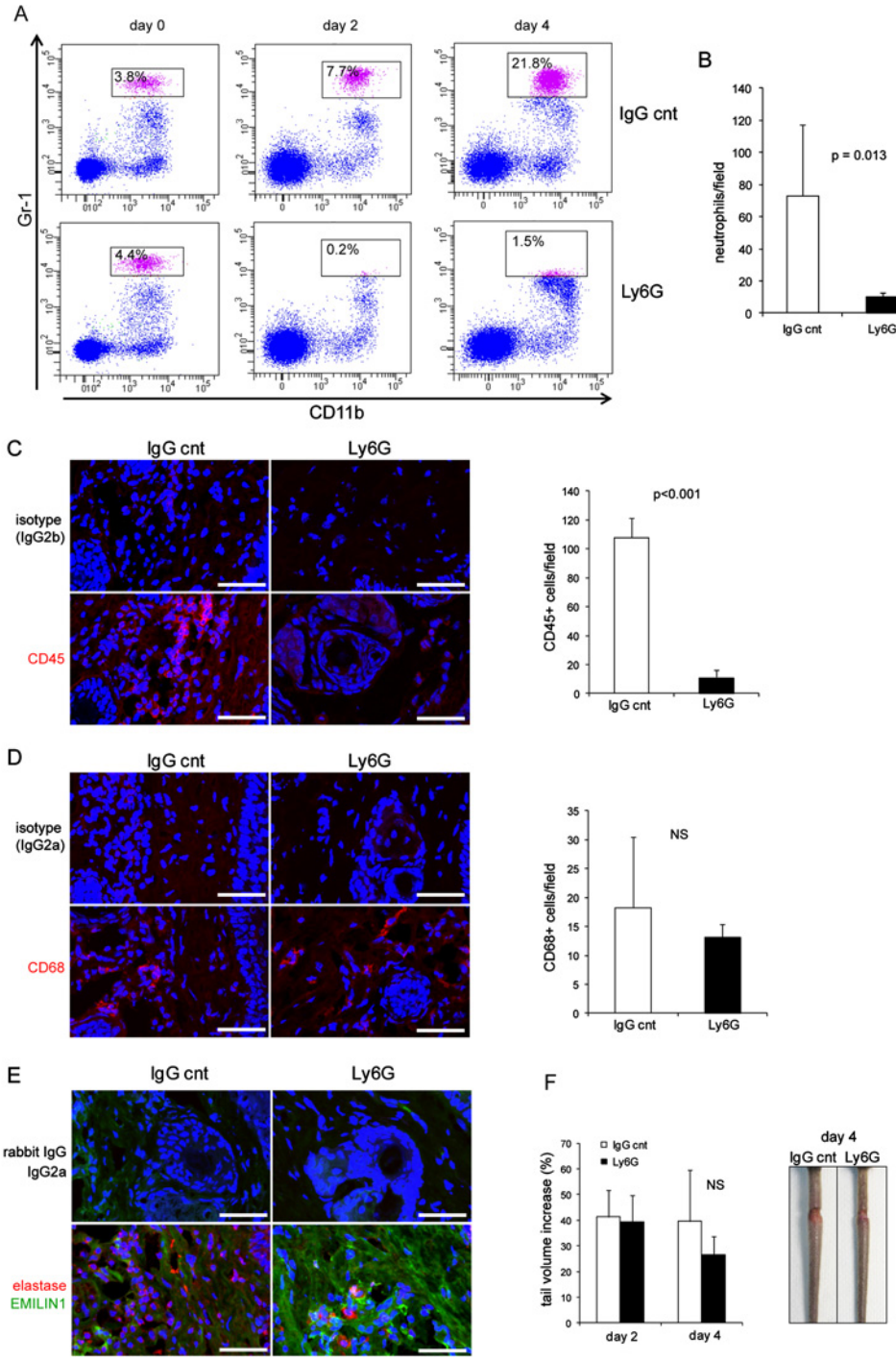

Figure 8 **Neutrophil depletion *in vivo* and swelling in tail lymphoedema model**

(**A**) Representative dot plots of neutrophils gated on CD45+ cells in blood of control (IgG cnt) and anti-Ly6G-treated recipient mice. $CD11b^{+}Gr1^{high}$ cells (boxed area) were identified as neutrophils. (**B**) Quantitative analysis of neutrophil numbers in H&E-stained tail sections 4 days after injury in control and anti-Ly6G-treated recipient mice. (**C**–**E**) Representative images of sections 4 days after injury in control and anti-Ly6G-treated recipient mice immunostained with (C) anti-CD45, (D) CD68, and (E) elastase and EMILIN1 antibodies. The graphs in (B–D) report the means±S.D.s obtained from four mice per group, analysing four fields (40×, original magnification) for each sample. (**F**) Anti-Ly6G-treated recipient mice showed a reduced but insignificant (NS) extent of swelling compared with the control mice 4 days after surgery. Scale bar = 50 μm.

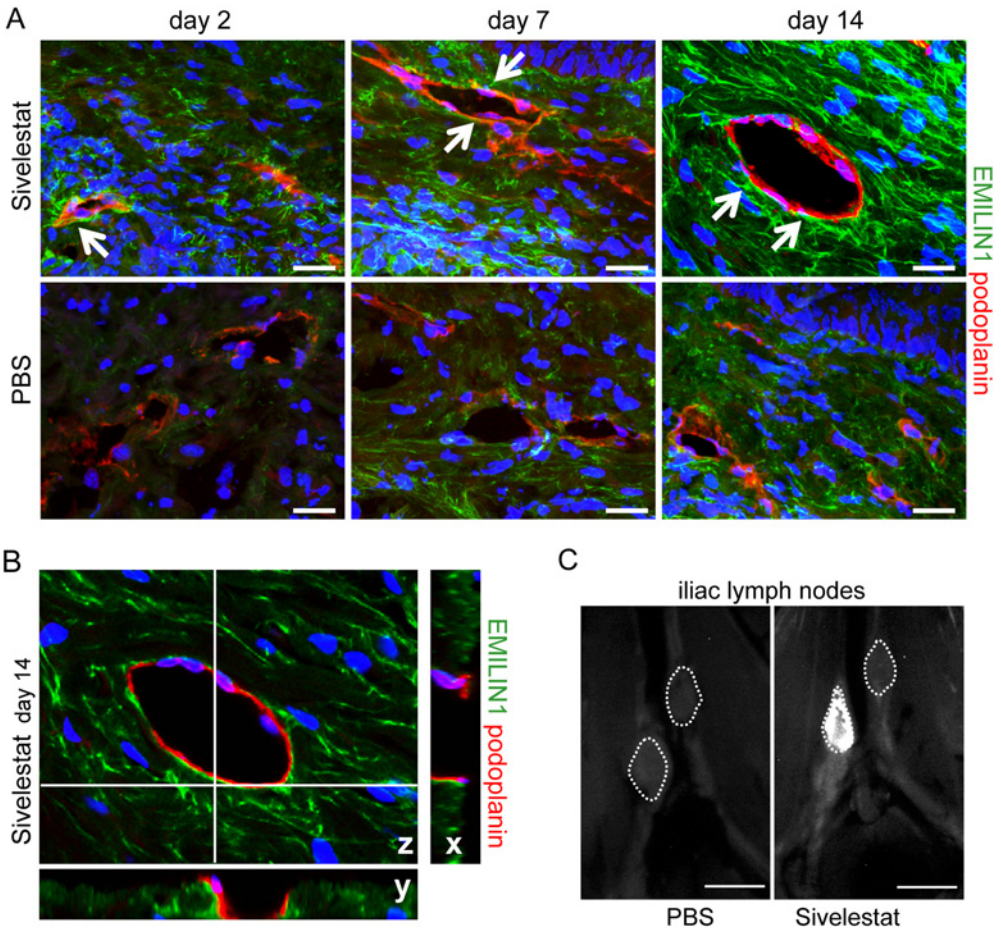

Figure 9 **Local treatment with sivelestat restores lymphatic functionality**

(**A**) EMILIN1 staining was highly reduced in PBS-treated mice even at day 7 after wounding, very probably because of degradation by NE, whereas in silvelestat-treated mice EMILIN1 fibres appeared to be well deposited and in close contact with lymphatic vessels (arrows). (**B**) The z-section of the sivelestat-treated tail at day 14 as reported in (A); the corresponding x and y projections clearly provide evidence for the close (yellow) association of EMILIN1 with lymphatic vessel cell membranes. (**C**) FITC–dextran was already drained by lymph nodes in sivelestat-treated but not control (PBS) mice at day 4 after surgery. Scale bars = 20 μm (A), 2 mm (C).

drained to lymph nodes in sivelestat-treated but not control mice (Figure 9C).

DISCUSSION

To the best of our knowledge, this is the first report to focus on the role of an ECM component in the pathogenesis of secondary lymphoedema. Most of the recent research has focused on the molecular basis of lymphatic development and generated several genetic animal models that are useful to identify key regulators of embryonic lymphatic development and provide insight into the mechanisms of primary lymphatic insufficiency [36]. The tissue responses to the interplay of local inflammation, matrix remodelling and lymphangiogenesis in secondary lymphatic insufficiency are less well understood. Inflammation triggers lymphangiogenesis [37,38], and various lymphangiogenic factors, such as VEGF-C, VEGF-D and hepatocyte growth factor, were identified as necessary to regulate lymphatic regeneration [39]. However, the crucial regulators in the coordination of the repair processes after lymphatic injury still need to be elucidated. Optimism over the promise of growth factor therapy for the treatment of secondary lymphoedema has been dampened [40,41]. Contrasting observations emerged to show that exogenous growth factor administration to sites of lymphatic injury augmented early LEC proliferation, but without the development of a functionally competent vasculature [42]. This was the case for delivery of exogenous VEGF-C [43], suggesting that VEGF-C/VEGF receptor-3 signalling may not be sufficient for the organizational evolution of lymphangiogenesis. Furthermore, it seems that the ability of the lymphatic vasculature to regenerate after injury is governed by a controlled balance between pro- and anti-lymphangiogenic cytokines [44]. In this context, the role of ECM has been poorly considered. The *Emilin1*$^{-/-}$ mouse model has represented the first abnormal lymphatic phenotype associated with deficiency

of an ECM protein, thus providing a unique and useful tool to demonstrate the role of a key structural element in the maintenance of lymphatic vessels' integrity and in regulation of lymphangiogenesis. Our previous studies, in fact, demonstrated that EMILIN1 genetic deficiency induces a significant reduction of AFs in the lymphatic capillaries [8], and unveiled EMILIN1 as a novel ligand for LEC α_9-integrin, suggesting that EMILIN1 played a direct role in growth and maintenance of lymphatic vessels [11].

In the present study, we propose EMILIN1 as a 'structural' regulator for a competent vasculature. Through use of a post-surgical tail lymphoedema model, we show that EMILIN1 degradation by NE is an early event in the pathogenesis of lymphoedema.

We also demonstrate that, in the first phases of the inflammatory process after tail surgery, the cellular infiltrate is mainly represented by neutrophils. It is well known that neutrophils synthesize a number of different proteases, including NE and MMP-8 and MMP-9 [45]. Among these enzymes, NE is the only one that can cleave EMILIN1 because sivelestat fully blocked the effect of lymph extracted from lymphoedematous tissues, whereas GM6001, a broad-spectrum MMP inhibitor, was totally ineffective. In a recent study, Rigby et al. [46] found that, during neutrophil transit of the inflamed lymphatic endothelium, MMP-8, MMP-9 and NE promote the endothelial retraction that increases junctional permeability, enabling neutrophil transmigration. They did not identify the substrates of the neutrophil enzymes, but hypothesized that ECM components were involved. The present study provides evidence that EMILIN1 is the elective ECM substrate, as demonstrated *in vitro* by experiments on the increased permeability of LECs after NE treatment and EMILIN1 degradation.

The crucial role of neutrophils in lymphoedema pathogenesis remains to be fully and well characterized. Our neutrophil depletion approach clearly demonstrated that it is necessary to fully inhibit NE to restore lymphatic endothelial functionality: the presence of few neutrophils after Ly6G treatment, but positivity for elastase staining, did not allow a strong and significant effect in reducing tail swelling.

In fact, only the treatment with sivelestat significantly inhibited the development of lymphoedema in the acute phase; in so doing it could also delay or even avoid the onset of the chronic phase. It is known that transforming growth factor (TGF)-β increases the tissue fibrosis that characterizes the chronic phase of lymphoedema and impairs lymphatic regeneration [47]. As the genetic inactivation of EMILIN1 causes increased TGF-β levels [12], it is reasonable to hypothesize that, in the absence of EMILIN1, as in *Emilin1*$^{-/-}$ mice (see Figure 1), or after its cleavage as in secondary lymphoedema, the lymphangiogenic response could also be altered via an indirect TGF-β-dependent mechanism.

The rationale for using sivelestat as a novel 'ECM' pharmacological approach to assess new lymphoedema treatments is highly supported by *ex vivo* analyses of human lymphoedema samples, in which few neutrophils were still present, even if among several cells typical of the chronic inflammatory process. Degraded EMILIN1 was, however, detected.

In summary, EMILIN1 is a structural element that assures a proper functionality of the LEC intercellular junctions. Thus, prevention of EMILIN1 cleavage in the acute phase of inflammation, by locally inhibiting the activity of NE, could be a powerful strategy to avoid lymphatic vessel impairment and the consequent severe development of secondary lymphoedema.

CLINICAL PERSPECTIVE

- As a therapeutically relevant treatment of secondary lymphoedema has yet to be achieved, the impact of lymphoedema remains a serious healthcare problem, above all in cancer patients. The role of ECM in lymphoedema still needs to be elucidated.
- We show that the degradation of the ECM protein EMILIN1 by NE is an early event in the acute phase of lymphoedema.
- The local administration of a specific elastase inhibitor prevents EMILIN1 degradation, reduces lymphoedema and restores lymphatic functionality, thus providing the rationale for a powerful strategy to avoid the consequent development of severe secondary lymphoedema.

AUTHOR CONTRIBUTION

Eliana Pivetta and Paola Spessotto conceived and designed the study; Eliana Pivetta, Bruna Wassermann, Carla Danussi, Lisa Del Bel Belluz, Teresa Maria Elisa Modica, Giulia Bosisio and Orlando Maiorani developed methodology and performed *in vitro* and *in vivo* experiments; Francesco Boccardo and Vincenzo Canzonieri provided and performed analyses on human lymphoedema samples; Alfonso Colombatti and Paola Spessotto reviewed and interpreted data; Eliana Pivetta and Paola Spessotto analysed data and supervised the study; Paola Spessotto wrote the manuscript. All authors read and approved the final manuscript.

ACKNOWLEDGEMENTS

We thank Gustavo Baldassarre for critical comments on the manuscript.

FUNDING

This work was supported by Associazione Italiana per la Ricerca sul Cancro (AIRC) [IG 14192] and the Ministry of Health [RF-2010–2309719].

REFERENCES

1 Alitalo, K., Tammela, T. and Petrova, T.V. (2005) Lymphangiogenesis in development and human disease. Nature **438**, 946–953 CrossRef PubMed

2 Gerli, R., Ibba, L. and Fruschelli, C. (1991) Ultrastructural cytochemistry of anchoring filaments of human lymphatic capillaries and their relation to elastic fibers. Lymphology **24**, 105–112 PubMed

3 De Cock, H.E., Affolter, V.K., Farver, T.B., Van, B.L., Scheuch, B. and Ferraro, G.L. (2006) Measurement of skin desmosine as an indicator of altered cutaneous elastin in draft horses with chronic progressive lymphedema. Lymphat. Res. Biol. **4**, 67–72 CrossRef PubMed

4 Rockson, S.G. (2012) Update on the biology and treatment of lymphedema. Curr. Treat. Options Cardiovasc. Med. **14**, 184–192 CrossRef PubMed

5 Witte, M.H., Bernas, M.J., Martin, C.P. and Witte, C.L. (2001) Lymphangiogenesis and lymphangiodysplasia: from molecular to clinical lymphology. Microsc. Res. Tech. **55**, 122–145 CrossRef PubMed

6 Colombatti, A., Bressan, G.M., Castellani, I. and Volpin, D. (1985) Glycoprotein 115, a glycoprotein isolated from chick blood vessels, is widely distributed in connective tissue. J. Cell Biol. **100**, 18–26 CrossRef PubMed

7 Colombatti, A., Poletti, A., Bressan, G.M., Carbone, A. and Volpin, D. (1987) Widespread codistribution of glycoprotein gp 115 and elastin in chick eye and other tissues. Coll. Relat. Res. **7**, 259–275 CrossRef PubMed

8 Danussi, C., Spessotto, P., Petrucco, A., Wassermann, B., Sabatelli, P., Montesi, M., Doliana, R., Bressan, G.M. and Colombatti, A. (2008) Emilin1 deficiency causes structural and functional defects of lymphatic vasculature. Mol. Cell Biol. **28**, 4026–4039 CrossRef PubMed

9 Danussi, C., Petrucco, A., Wassermann, B., Pivetta, E., Modica, T.M., Belluz, L.B., Colombatti, A. and Spessotto, P. (2011) EMILIN1-α4/α9 integrin interaction inhibits dermal fibroblast and keratinocyte proliferation. J. Cell Biol. **195**, 131–145 CrossRef PubMed

10 Spessotto, P., Cervi, M., Mucignat, M.T., Mungiguerra, G., Sartoretto, I., Doliana, R. and Colombatti, A. (2003) β_1-Integrin-dependent cell adhesion to EMILIN-1 is mediated by the gC1q domain. J. Biol. Chem. **278**, 6160–6167 CrossRef PubMed

11 Danussi, C., Del Bel, B.L., Pivetta, E., Modica, T.M., Muro, A., Wassermann, B., Doliana, R., Sabatelli, P., Colombatti, A. and Spessotto, P. (2013) EMILIN1/alpha9beta1 integrin interaction is crucial in lymphatic valve formation and maintenance. Mol. Cell Biol. **33**, 4381–4394 CrossRef PubMed

12 Zacchigna, L., Vecchione, C., Notte, A., Cordenonsi, M., Dupont, S., Maretto, S., Cifelli, G., Ferrari, A., Maffei, A., Fabbro, C. et al. (2006) Emilin1 links TGF-beta maturation to blood pressure homeostasis. Cell **124**, 929–942 CrossRef PubMed

13 Zanetti, M., Braghetta, P., Sabatelli, P., Mura, I., Doliana, R., Colombatti, A., Volpin, D., Bonaldo, P. and Bressan, G.M. (2004) EMILIN-1 deficiency induces elastogenesis and vascular cell defects. Mol. Cell Biol. **24**, 638–650 CrossRef PubMed

14 Swartz, M.A., Kaipainen, A., Netti, P.A., Brekken, C., Boucher, Y., Grodzinsky, A.J. and Jain, R.K. (1999) Mechanics of interstitial-lymphatic fluid transport: theoretical foundation and experimental validation. J. Biomech. **32**, 1297–1307 CrossRef PubMed

15 Jin, da P., An, A., Liu, J., Nakamura, K. and Rockson, S.G. (2009) Therapeutic responses to exogenous VEGF-C administration in experimental lymphedema: immunohistochemical and molecular characterization. Lymphat. Res. Biol. **7**, 47–57 CrossRef PubMed

16 Tammela, T., Saaristo, A., Holopainen, T., Lyytikka, J., Kotronen, A., Pitkonen, M., Abo-Ramadan, U., Yla-Herttuala, S., Petrova, T.V. and Alitalo, K. (2007) Therapeutic differentiation and maturation of lymphatic vessels after lymph node dissection and transplantation. Nat. Med. **13**, 1458–1466 CrossRef PubMed

17 Saaristo, A., Karkkainen, M.J. and Alitalo, K. (2002) Insights into the molecular pathogenesis and targeted treatment of lymphedema. Ann. N. Y. Acad. Sci. **979**, 94–110 CrossRef PubMed

18 Tervala, T.V., Hartiala, P., Tammela, T., Visuri, M.T., Yla-Herttuala, S., Alitalo, K. and Saarikko, A.M. (2015) Growth factor therapy and lymph node graft for lymphedema. J. Surg. Res. **196**, 200–207 CrossRef PubMed

19 Nakamura, K., Radhakrishnan, K., Wong, Y.M. and Rockson, S.G. (2009) Anti-inflammatory pharmacotherapy with ketoprofen ameliorates experimental lymphatic vascular insufficiency in mice. PLoS One **4**, e8380 CrossRef PubMed

20 Tabibiazar, R., Cheung, L., Han, J., Swanson, J., Beilhack, A., An, A., Dadras, S.S., Rockson, N., Joshi, S., Wagner, R. et al. (2006) Inflammatory manifestations of experimental lymphatic insufficiency. PLoS Med **3**, e254 CrossRef PubMed

21 Casley-Smith, J.R. (1999) Benzo-pyrones in the treatment of lymphoedema. Int. Angiol. **18**, 31–41 PubMed

22 Badger, C., Preston, N., Seers, K. and Mortimer, P. (2004) Benzo-pyrones for reducing and controlling lymphoedema of the limbs. Cochrane Database Syst. Rev. CD003140 PubMed

23 Pivetta, E., Danussi, C., Wassermann, B., Modica, T.M., Del Bel, B.L., Canzonieri, V., Colombatti, A. and Spessotto, P. (2014) Neutrophil elastase-dependent cleavage compromises the tumor suppressor role of EMILIN1. Matrix Biol **34**, 22–32 CrossRef PubMed

24 Mongiat, M., Mungiguerra, G., Bot, S., Mucignat, M.T., Giacomello, E., Doliana, R. and Colombatti, A. (2000) Self-assembly and supramolecular organization of EMILIN. J. Biol. Chem. **275**, 25471–25480 CrossRef PubMed

25 Sitzia, J. (1995) Volume measurement in lymphoedema treatment: examination of formulae. Eur. J. Cancer Care (Engl.) **4**, 11–16 CrossRef PubMed

26 Mancardi, S., Stanta, G., Dusetti, N., Bestagno, M., Jussila, L., Zweyer, M., Lunazzi, G., Dumont, D., Alitalo, K. and Burrone, O.R. (1999) Lymphatic endothelial tumors induced by intraperitoneal injection of incomplete Freund's adjuvant. Exp. Cell Res. **246**, 368–375 CrossRef PubMed

27 Danussi, C., Petrucco, A., Wassermann, B., Modica, T.M., Pivetta, E., Del Bel, B.L., Colombatti, A. and Spessotto, P. (2012) An EMILIN1-negative microenvironment promotes tumor cell proliferation and lymph node invasion. Cancer Prev. Res. (Phila) **5**, 1131–1143 CrossRef PubMed

28 Boccardo, F., Fulcheri, E., Villa, G., Molinari, L., Campisi, C., Dessalvi, S., Murdaca, G., Campisi, C., Santi, P.L., Parodi, A. et al. (2013) Lymphatic microsurgery to treat lymphedema: techniques and indications for better results. Ann. Plast. Surg. **71**, 191–195 CrossRef PubMed

29 Sopracordevole, F., Mancioli, F., Canzonieri, V., Buttignol, M., Giorda, G. and Ciavattini, A. (2015) Laser CO treatment for vulvar lymphedema secondary to gynecological cancer therapy: a report of two cases and review of the literature. Oncol. Lett. **9**, 1889–1892 PubMed

30 Sun, M., Fu, H., Cheng, H., Cao, Q., Zhao, Y., Mou, X., Zhang, X., Liu, X. and Ke, Y. (2012) A dynamic real-time method for monitoring epithelial barrier function in vitro. Anal. Biochem. **425**, 96–103 CrossRef PubMed

31 Xing, J.Z., Zhu, L., Jackson, J.A., Gabos, S., Sun, X.J., Wang, X.B. and Xu, X. (2005) Dynamic monitoring of cytotoxicity on microelectronic sensors. Chem. Res. Toxicol. **18**, 154–161 CrossRef PubMed

32 Feng, L., Zhu, W., Huang, C. and Li, Y. (2012) Direct interaction of ONO-5046 with human neutrophil elastase through ^{1}H NMR and molecular docking. Int. J. Biol. Macromol. **51**, 196–200 CrossRef PubMed

33 Wang, Z.Q., Chen, L.Q., Yuan, Y., Wang, W.P., Niu, Z.X., Yang, Y.S. and Cai, J. (2015) Effects of neutrophil elastase inhibitor in patients undergoing esophagectomy: a systematic review and meta-analysis. World J. Gastroenterol. **21**, 3720–3730 CrossRef PubMed

34 Tagami, T., Tosa, R., Omura, M., Fukushima, H., Kaneko, T., Endo, T., Rinka, H., Murai, A., Yamaguchi, J., Yoshikawa, K. et al. (2014) Effect of a selective neutrophil elastase inhibitor on mortality and ventilator-free days in patients with increased extravascular lung water: a post hoc analysis of the PiCCO Pulmonary Edema Study. J. Intensive Care **2**, 67 CrossRef PubMed

35 Henriksen, P.A. (2014) The potential of neutrophil elastase inhibitors as anti-inflammatory therapies. Curr. Opin. Hematol. **21**, 23–28 CrossRef PubMed

36 Eklund, L., Bry, M. and Alitalo, K. (2013) Mouse models for studying angiogenesis and lymphangiogenesis in cancer. Mol. Oncol. **7**, 259–282 CrossRef PubMed

37 Kim, H., Kataru, R.P. and Koh, G.Y. (2014) Inflammation-associated lymphangiogenesis: a double-edged sword? J. Clin. Invest **124**, 936–942 CrossRef

38 Liao, S. and von der Weid, P.Y. (2014) Inflammation-induced lymphangiogenesis and lymphatic dysfunction. Angiogenesis **17**, 325–334 CrossRef PubMed

39 Shin, W.S. and Rockson, S.G. (2008) Animal models for the molecular and mechanistic study of lymphatic biology and disease. Ann. N. Y. Acad. Sci. **1131**, 50–74 CrossRef PubMed

40 Goldman, J., Rutkowski, J.M., Shields, J.D., Pasquier, M.C., Cui, Y., Schmokel, H.G., Willey, S., Hicklin, D.J., Pytowski, B. and Swartz, M.A. (2007) Cooperative and redundant roles of VEGFR-2 and VEGFR-3 signaling in adult lymphangiogenesis. FASEB J. **21**, 1003–1012 CrossRef PubMed

41 Rutkowski, J.M., Boardman, K.C. and Swartz, M.A. (2006) Characterization of lymphangiogenesis in a model of adult skin regeneration. Am. J. Physiol Heart Circ. Physiol. **291**, H1402–H1410 CrossRef PubMed

42 Rutkowski, J.M., Moya, M., Johannes, J., Goldman, J. and Swartz, M.A. (2006) Secondary lymphedema in the mouse tail: Lymphatic hyperplasia, VEGF-C upregulation, and the protective role of MMP-9. Microvasc. Res. **72**, 161–171 CrossRef PubMed

43 Goldman, J., Le, T.X., Skobe, M. and Swartz, M.A. (2005) Overexpression of VEGF-C causes transient lymphatic hyperplasia but not increased lymphangiogenesis in regenerating skin. Circ. Res. **96**, 1193–1199 CrossRef PubMed

44 Zampell, J.C., Avraham, T., Yoder, N., Fort, N., Yan, A., Weitman, E.S. and Mehrara, B.J. (2012) Lymphatic function is regulated by a coordinated expression of lymphangiogenic and anti-lymphangiogenic cytokines. Am. J. Physiol Cell Physiol. **302**, C392–C404 CrossRef PubMed

45 Nathan, C. (2006) Neutrophils and immunity: challenges and opportunities. Nat. Rev. Immunol. **6**, 173–182 CrossRef PubMed

46 Rigby, D.A., Ferguson, D.J., Johnson, L.A. and Jackson, D.G. (2015) Neutrophils rapidly transit inflamed lymphatic vessel endothelium via integrin-dependent proteolysis and lipoxin-induced junctional retraction. J. Leukoc. Biol. **98**, 897–912 CrossRef PubMed

47 Avraham, T., Daluvoy, S., Zampell, J., Yan, A., Haviv, Y.S., Rockson, S.G. and Mehrara, B.J. (2010) Blockade of transforming growth factor-beta1 accelerates lymphatic regeneration during wound repair. Am. J. Pathol. **177**, 3202–3214 CrossRef PubMed

Received 22 September 2015; accepted 26 February 2016

Accepted Manuscript online 26 February 2016, doi: 10.1042/CS20160064